ChemComm
Chemical Communications

Accepted Manuscript

This article can be cited before page numbers have been issued, to do this please use: G. A. Volpato, M. Marasi, T. Gobbato, F. Valentini, F. Sabuzi, V. Gagliardi, A. Bonetto, A. Marcomini, S. Berardi, V. Conte, M. Bonchio, S. Caramori, P. Galloni and A. Sartorel, *Chem. Commun.*, 2020, DOI: 10.1039/C9CC09805D.

ROYAL SOCIETY OF CHEMISTRY

rsc.li/chemcomm

View Article Online
DOI: 10.1039/C9CC09805D

COMMUNICATION

Photoanodes for water oxidation with visible light based on a pentacyclic quinoid organic dye enabling proton-coupled electron transfer†

T5ytReceived 00th January 20xx,
Accepted 00th January 20xx

DOI: 10.1039/x0xx00000x

Giulia Alice Volpato,[a‖] Martina Marasi, [a,b‖] Thomas Gobbato, [a] Francesca Valentini, [b] Federica Sabuzi,[b] Valeria Gagliardi,[a,b] Alessandro Bonetto,[c] Antonio Marcomini,[c] Serena Berardi,*[d] Valeria Conte,[b] Marcella Bonchio,[a] Stefano Caramori,[d] Pierluca Galloni*[b] and Andrea Sartorel*[a]

A pentacyclic quinoid dye, KuQ(O)$_3$OH, combining (i) extended visible absorption up to 600 nm, (ii) excited state reduction potential > 2 V vs NHE, (iii) photoinduced proton coupled electron transfer mechanism, has been used for the fabrication of dye-sensitized SnO_2 photoanodes integrating a ruthenium polyoxometalate water oxidation catalyst. The resulting photoelectrodes SnO_2|KuQ(O)$_3$OH|Ru$_4$POM display a Light Harvesting Efficiency up to 90% in the range 500 – 600 nm, onset potential as low as of 0.2 V vs NHE at pH 5.8, photoinduced oxygen evolution with faradaic efficiency 70±15% and absorbed-photon-to-current efficiency up to 0.12±0.01%.

Photoelectrochemical cells (PECs) are a promising technology for converting solar energy into chemical fuels, i.e. by means of light induced water splitting.[1] The development of dye-sensitized photoelectrodes for PECs is one of the current strategies to exploit solar radiation in the visible region.[2] Photoanodes for water oxidation have been developed with dyes comprising ruthenium(II) polypyridine derivatives,[3] porphyrinoids,[4] BODIPY,[5] perylenes,[6] polymeric films,[7] triarylamines.[8] In particular, the use of molecularly defined organic chromophores provides the advantages of tuning the spectroscopic and redox properties, while avoiding the use of rare transition metals.[2,4-8]

In this work, we exploit a pentacyclic quinoid organic dye[9] 1-(3-carboxypropyl)KuQuinone (KuQ(O)$_3$OH) anchored onto nanostructured tin oxide semiconductor to achieve photoelectrochemical water oxidation, when integrated with a ruthenium polyoxometalate catalyst (Ru$_4$POM),[6d,10a] scheme 1. Besides being a novel class of dyes for this application, two significant features distinguish KuQ(O)$_3$OH from the pool already developed in literature: (i) the ability to manage proton coupled electron transfer (PCET), which is a peculiar feature of water oxidation photosynthetic schemes[11] and (ii) a "non-classical" mechanism, based on the reductive quenching of the excited state of the dye, followed by electron injection into the semiconductor conduction band.

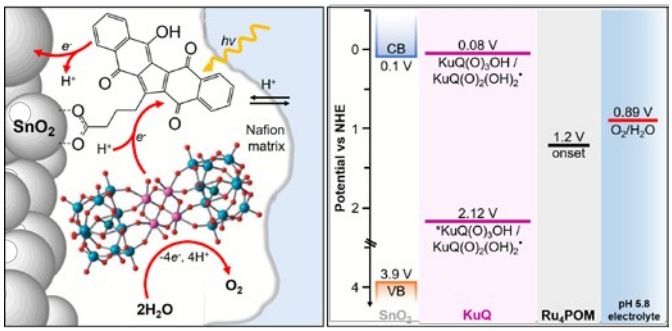

Scheme 1. Schematic representation of SnO_2|KuQ(O)$_3$OH|Ru$_4$POM photoanodes for water oxidation. The energy levels are shown for the system at pH = 5.8.

KuQuinone dyes show extended absorption in the visible region.[9] In tetrahydrofurane solution, KuQ(O)$_3$OH presents two intense absorption maxima (λ_1 = 563 nm, ε^{563} = 1.5 × 10^4 M^{-1} cm^{-1}; λ_2 = 529 nm, ε^{529} = 1.17 × 10^4 M^{-1} cm^{-1}), redshifted with respect to those observed for the deprotonated enolate KuQ(O)$_3$O$^-$ (λ_1 =534 nm, ε^{534} =7.2 × 10^3 M^{-1} cm^{-1}; λ_2 = 504 nm ε^{504} =8.4 × 10^3 M^{-1} cm^{-1}), Figure S1 in ESI. Time-dependent density functional calculations at B3LYP/6-31g+(d,p) level of theory, including a polarizable continuum model of the solvent, assign the lowest energy absorption bands to HOMO→LUMO transitions, with both orbitals delocalized on the extended aromatic scaffold (Figure S2 in ESI).[9] The emission properties of the dye are influenced by the acid base equilibria occurring at the ground and excited states. Emission spectra show broad bands with maxima in the range 560–600 nm (quantum yields 1.1–7.9%), decaying with lifetimes of 0.63-3.57 ns, consistent with singlet excited states (Figures S3-S4 in ESI). From the intersection of the normalized absorption and

[a] Department of Chemical Sciences, University of Padova, via Marzolo 1 35131 Padova (Italy). E-mail: andrea.sartorel@unipd.it
[b] Department of Chemical Science and Technologies , University of Rome "Tor Vergata", via della Ricerca Scientifica, snc 00133 Roma, Italy. galloni@scienze.uniroma2.it
[c] Dept. Environmental Sciences, Informatics and Statistics, University Ca' Foscari Venice, Vegapark, Via delle Industrie 21/8, 30175 Marghera, Venice, Italy.
[d] Department of Chemical and Pharmaceutical Sciences, University of Ferrara, and Centro Interuniversitario per la Conversione Chimica dell'Energia Solare (SolarChem), sez. di Ferrara, Via L. Borsari 46, 44121 Ferrara, Italy. brrsrn@unife.it
‖ These authors equally contributed.
†Electronic Supplementary Information (ESI) available: Full experimental procedures, additional characterization of the dye and of the photoelectrodes. See DOI: 10.1039/x0xx00000x

emission, it is possible to estimate $E^{0\text{-}0}$ energy of 2.16 eV and 2.28 eV for $KuQ(O)_3OH$ and $KuQ(O)_3O^-$, respectively, and $E^{0\text{-}0} \approx$ 2.04 eV when the dye is anchored onto SnO_2 under the operative conditions employed in this work (pH 5.8), *vide infra*. Notably, the reduction potential of $KuQ(O)_3OH$ drop-cast onto glassy carbon electrode falls in the range 0.116 – 0.078 V vs NHE in aqueous electrolyte (0.1 M $Na_2SiF_6/NaHCO_3$ buffer, pH in the range 5.2-5.9),¶ and depends on pH with a slope of 58±1 mV per unit, indicative of a PCET involving a $KuQ(O)_3OH/KuQ(O)_2(OH)_2^\bullet$ couple (Figure 1a and Figure S6 in ESI).¥ Merging the electrochemical properties and the $E^{0\text{-}0}$ energy of 2.04 eV previously determined, the reduction potential of the excited state ($^*KuQ(O)_3OH/KuQ(O)_2(OH)_2^\bullet$ couple) stands in the range +2.12 to +2.16 V vs NHE.[12] Thus, the $^*KuQ(O)_3OH$ excited state is a very powerful oxidant, to be considered for application in photoelectrochemical oxidation of water (E = 0.89 V vs NHE at pH 5.8 for O_2/H_2O couple, scheme 1, right). In addition, the LUMO energy level is suitable for coupling the $KuQ(O)_3OH$ dye with semiconductors such as SnO_2 (conduction band at + 0.1 V vs NHE, scheme 1, right).[13]

Grafting of $KuQ(O)_3OH$ onto nanostructured SnO_2 was achieved by soaking the electrode overnight into a 0.13 mM solution of $KuQ(O)_3OH$ in tetrahydrofurane. The carboxylate function in the lateral chain allows to reach a notable surface loading of 140±20 nmol cm^{-2} (see ESI).‡ The absorbance spectra of $SnO_2|KuQ(O)_3OH$ photoanodes show the fingerprint of the dye, with a light harvesting efficiency (LHE) of ca 90% in the range 500 – 600 nm (Figure 1b). The photoelectrochemical properties of $SnO_2|KuQ(O)_3OH$ were tested by linear sweep voltammetry (LSV) in aqueous 0.1 M ascorbate electron donor at pH = 5.8 (i.e., the same pH used in photoelectrochemical water oxidation, *vide infra*), in order to verify the ability of the dye to inject electrons into the semiconductor, evaluating the onset potential and photocurrent density, together with the operating mechanism.♣ Comparing the LSV scans under dark and irradiation conditions, the raising of photocurrent is observed at an onset potential of 0.1 V vs NHE, reaching a photocurrent plateau of 0.4 mA/cm^2 at ca. 0.4 V (Fig. 1c; at E > 0.2 V a dark current due to oxidation of ascorbate is also observed). Transient absorption spectroscopy (TAS) experiments evidence the formation of the $KuQ(O)_2(OH)_2^\bullet$ reduced form of the dye, associated to the long-living absorption at λ > 610 nm (> 1.5 μs Figure 1d; this assignment is corroborated by the comparison with the TAS spectra obtained for the $KuQ(O)_3OH$ dye in THF solution containing ascorbate, Figure S8 in ESI). Therefore, the mechanism under these conditions is based on the dye excitation and subsequent reductive quenching of the $^*KuQ(O)_3OH$ excited state by the ascorbate donor to form the reduced $KuQ(O)_2(OH)_2^\bullet$, which is then responsible for electron injection into the conduction band of SnO_2 (Scheme 1).

These results prompted us to combine the $SnO_2|KuQ(O)_3OH$ electrodes with a tetraruthenium polyoxometalate water oxidation catalyst $Na_{10}\{Ru_4(\mu\text{-}O)_4(\mu\text{-}OH)_2[\gamma\text{-}SiW_{10}O_{36}]_2\}$, hereafter Ru_4POM (see CV in Figure S9),[10] that was already exploited in photoelectrodes with Ru polypyridine [10b,c] and perylene bisimide chromophores.[6d] Functionalization of $SnO_2|KuQ(O)_3OH$ electrodes with Ru_4POM was achieved by 30 minutes soaking into a 4 mM aqueous solution of Ru_4POM containing 1% v/v of Nafion polymer,[14] followed by rinsing in water (13±5 nmol cm^{-2} loading of Ru_4POM as revealed by inductively coupled plasma mass spectrometry, ICP-MS).♦

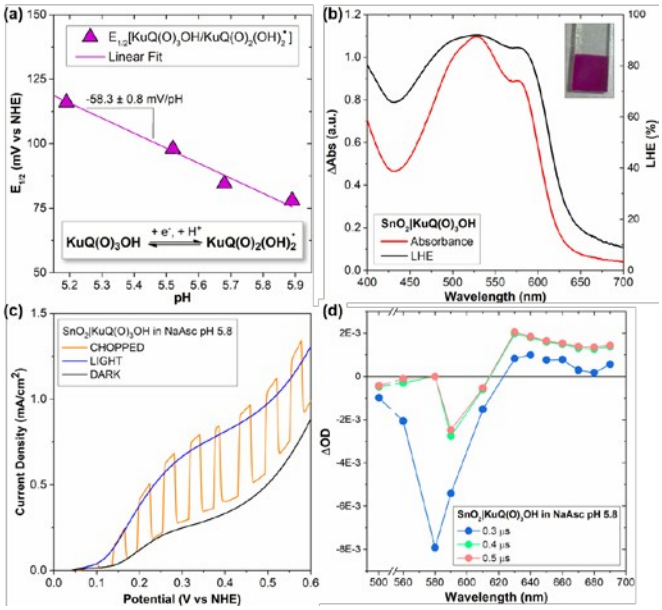

Figure 1. **(a)** Plot of $E_{1/2}$ vs pH for the $KuQ(O)_3OH/KuQ(O)_2(OH)_2^\bullet$. Inset: scheme of proton coupled electron transfer associated to the dye. **(b)** Absorption spectra and light harvesting efficiency (LHE) of $SnO_2|KuQ(O)_3OH$ photoanodes, after subtraction of SnO_2 contribution. Inset: photograph of the $SnO_2|KuQ(O)_3OH$ photoanode. **(c)** LSV registered for $SnO_2|KuQ(O)_3OH$ in sodium ascorbate 0.1 M at pH = 5.8 under dark and light conditions and under chopped irradiation (CE: Pt; RE: Ag/AgCl 3M NaCl; 20 mV s^{-1}; iR drop compensated, see section 2.5 in ESI; light: AM 1.5G + 400 nm cut-off filter). **(d)** Transient absorption spectra of a $SnO_2|KuQ(O)_3OH$ at different time delays after the 532 nm ns-laser excitation pulse, recorded in 1 M sodium ascorbate at pH = 5.8.

Absorption spectra of the $SnO_2|KuQ(O)_3OH|Ru_4POM$ photoanodes (Figure S10 in ESI) show an overall enhanced absorption in the visible region, consistent with the absorption features of Ru_4POM. Atomic Force Microscopy (AFM) and Scanning Electron Microscopy (SEM) images (Figures 2a, S11 and S12) reveal a smoothing of the surface with respect to $SnO_2|KuQ(O)_3OH$ electrodes, ascribable to the presence of the Nafion polymer. EDX elemental mapping (Figures S13 and S14) evidence the homogenous distribution of Ru_4POM and Nafion over the surface and, more importantly, through the whole 3 μm-thick layer of mesoporous SnO_2.

LSV experiments under dark and light conditions with $SnO_2|KuQ(O)_3OH|Ru_4POM$ electrodes are reported in figure 2b.# The dark scan (black trace) shows an initial dark current density, stabilizing at ca 10 μA cm^{-2} at potentials > 0.6 V vs NHE (corresponding to 0.95 V vs Reversible Hydrogen Electrode, RHE). This dark current contribution, occurring at potentials far below the one of the dark water oxidation process (E = 1.23 V vs RHE) and not associated to oxygen evolution, is originated by the re-oxidation of Sn(III) generated when the cell is switched on at potentials corresponding to the Sn(IV)/(III) process, and by redox processes of Ru_4POM (Figure S9 in ESI); a further capacitive contribution arises from the presence of

the Nafion layer. Under irradiation (blue trace and chopped orange trace), a photocurrent is observed starting at a low onset potential of 0.20 V vs NHE (0.55 V vs RHE), while reaching a net and constant value of 20 μA cm^2 in the range 0.4 – 1 V vs NHE (0.75 – 1.35 V vs RHE). The attribution of the observed photocurrent to oxygen evolution was confirmed through a generator-collector (G-C) method, where the anodic photocurrent produced at the $SnO_2|KuQ(O)_3OH|Ru_4POM$ generator held at 0.8 V vs NHE (1.15 V vs RHE), is accompanied by a cathodic current of oxygen reduction at a FTO collector, held at -0.7 V vs NHE (Figure 2c, see the Methods section and Figures S15-S16 in ESI).[6d,15] A Faradaic efficiency for photoinduced oxygen evolution of 70±15 % was thus estimated (see Table S2 in ESI). Conversely, in the case of catalyst-free $SnO_2|KuQ(O)_3OH$ electrodes (stationary photocurrent of ca 8 μA), no significant cathodic current for oxygen reduction is produced (Figure S17), confirming the fundamental role of Ru_4POM in driving water oxidation.

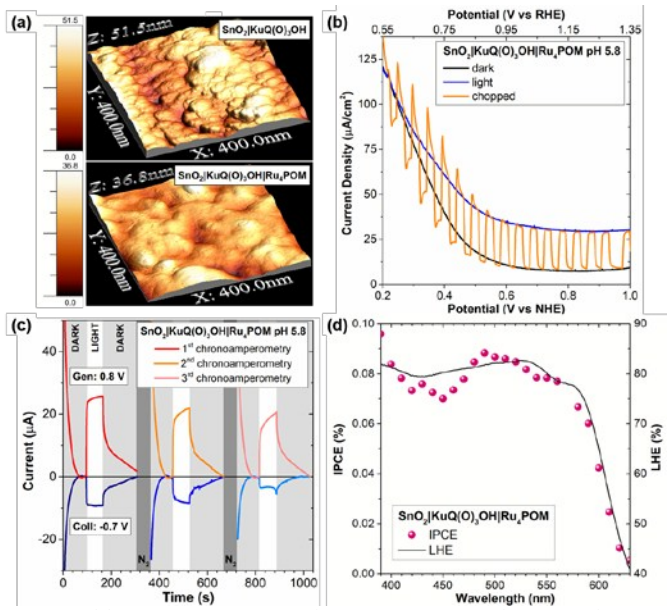

Figure 2. **(a)** AFM images of $SnO_2|KuQ(O)_3OH$ and $SnO_2|KuQ(O)_3OH|Ru_4POM$ photonodes. **(b)** LSV for $SnO_2|KuQ(O)_3OH|Ru_4POM$ in 0.1 M $Na_2SiF_6/NaHCO_3$ buffer pH 5.8 (CE: Pt; RE: Ag/AgCl 3M NaCl; 20 mV s^{-1}; light: AM 1.5G + 400 nm cut-off filter). **(c)** Consecutive G-C experiments for O_2 detection with $SnO_2|KuQ(O)_3OH|Ru_4POM$ in 0.1 M $Na_2SiF_6/NaHCO_3$ buffer pH 5.8; the positive photocurrent (red, orange, pink traces) is accompanied by a negative current of O_2 reduction at the FTO collector (blue, light blue, azure traces); CE: Pt; RE: Ag/AgCl 3M NaCl; light: white LED + 400 nm cut-off filter, see ESI. **(d)** IPCE (purple dots) obtained in $Na_2SiF_6/NaHCO_3$ buffer pH 5.8 and light harvesting efficiency (black line) of $SnO_2|KuQ(O)_3OH|Ru_4POM$

The Incident Photon-to-Current Efficiency (IPCE) reflects remarkably well the absorption spectrum of the photoanode, with a peak value of 0.09 % at 490 nm (Figure 2d). This value is similar to those obtained with KuQuinone derivatives deposited onto flat ITO substrates, in the presence of amines as sacrificial electron donors.[9d] The internal quantum efficiency (Absorbed Photon-to-Current Efficiency, APCE=IPCE/LHE) is nearly constant in the 400 – 550 nm region of the spectrum, with an average value around 0.12±0.01%. Benchmark metrics for dye-sensitized photoanodes for water oxidation are reported in table S3 in ESI; in this scenario, $SnO_2|KuQ(O)_3OH|Ru_4POM$ electrodes are characterized by a low onset potential, while reaching photocurrent density, Faradaic efficiency and IPCE/APCE observed for electrodes sensitized with engineered Ru(II) polypyridine chromophores and the same Ru_4POM catalyst.

The charge transfer dynamics were preliminary investigated by TAS. However, traces obtained for $SnO_2|KuQ(O)_3OH|Ru_4POM$ did not reveal diagnostic transient absorption features, and thus were poorly informative. The dye and catalyst were then assembled on insulating ZrO_2 films, characterised by a high energy conduction band that precludes electron injection, in order to favour the accumulation of stationary intermediates. For $ZrO_2|KuQ(O)_3OH$, laser irradiation led to the formation of a transient absorption decaying in several μs (Figure S18): this is ascribable to the lowest triplet excited state of $KuQ(O)_3OH$, populated by intersystem crossing from the singlet excited state, in the absence of quenching species. Conversely, in $ZrO_2|KuQ(O)_3OH|Ru_4POM$, the absence of such long lived dynamics suggests a fast evolution of the dye excited state in the presence of Ru_4POM, and likely involving a charge transfer from Ru_4POM to $^*KuQ(O)_3OH$, forming oxidized Ru_4POM and reduced $KuQ(O)_2(OH)_2^{\bullet}$. However, no features of this charge separated state is observed in the ns-μs domain, as the result of fast recombination, that may thus limit the overall quantum efficiency under photoelectrochemical conditions.

Concerning stability, a decrease of photocurrent density was observed during 90 minutes of photoelectrolysis, with a drop to 60% of the initial value after 30 minutes, and to ca 30% after 90 minutes (Fig. S19 in ESI). This is associated to a visible leaching of $KuQ(O)_3OH$ dye and Ru_4POM catalyst from the electrode: 1.75±0.25 nmol/cm^2 of Ru_4POM were quantified by ICP-MS on the stressed electrodes, accounting for 13% of the initial loading; a further engineering of the photoanode is thus required to improve long term stability, which is however a diffuse issue in molecular based photoanodes.[3-8]

In conclusion, we have reported novel photoanodes for water oxidation based on an organic quinoid dye, with a strong absorption in the visible (up to 600 nm, $\varepsilon \approx 1.5 \times 10^4$ M^{-1}cm^{-1}), having a highly oxidizing excited state (E > 2 V vs NHE) and capable of promoting photoinduced proton coupled electron transfer. The $SnO_2|KuQ(O)_3OH|Ru_4POM$ perform photoelectrochemical water oxidation at a low onset potential, with Faradaic efficiency of 70±15%, IPCE and APCE values of 0.09% and 0.12±0.01%, respectively. These results offer a new possibility for the design and realization of dye-sensitized devices for photocatalytic applications.

This work was supported by the Department of Chemical Sciences at the University of Padova (P-DISC "Phoetry" #10BIRD2018-UNIPD) and by Fondazione Cariparo ("Synergy", Progetti di Eccellenza 2018). V.G. thanks Regione Lazio for a scholarship (Project "TornoSubito"). We thank Sara Bonacchi for assistance in spectroscopic characterization of $KuQ(O)_3OH$.

Conflicts of interest

There are no conflicts to declare.

Notes and references

¶ The Na_2SiF_6/$NaHCO_3$ buffer has been largely used in light driven water oxidation, and resulted the optimum choice for homogeneous systems employing Ru_4POM, see ref. 16.
¥ A second reversible wave is observed at ca 0.2 V more negative potentials, and attributed to the deprotonated dye involving the $KuQ(O)_3O^-$/$KuQ(O)_3OH^{\bullet-}$ couple (Figure S6 in ESI).
‡ After the sensitization procedure, the photoanodes present an intense orange colour ascribed to the deprotonated $KuQ(O)_3O^-$, and likely originated from acid/base reaction with the SnO_2 surface. Dipping the electrodes in aqueous sulfuric acid (pH 2) leads to a colour change to deep violet, typical of $KuQ(O)_3OH$. This treatment significantly enhances the stability of SnO_2|$KuQ(O)_3OH$ in water up to several hours.
♣ Photocurrent densities of 20-30 $\mu A/cm^2$ were observed with Br^- and triethanolamine donors in acidic and alkaline conditions, respectively, see Table S1 and Figure S7 in ESI.
♦ In the absence of Nafion, a lower loading of 5±1 $nmol/cm^{-2}$ Ru_4POM was obtained, with its immediate leaching when the electrodes were dipped in aqueous solution.
Under these conditions, the electrode remains deep violet, indicative of the persistence of the $KuQ(O)_3OH$ form.

1 (a) K. Park, Y. J. Kim, T. Yoon, S. David and Y. M. Song, *RSC Adv.*, 2019, **9**, 30112–30124; (b) L. Steier and S. Holliday, *J. Mater. Chem. A*, 2018, **6**, 21809–21826; (c) J. R. McKone, N. S. Lewis and H. B. Gray, *Chem. Mater.*, 2014, **26**, 407–414.

2 (a) J. T. Kirner and R. G. Finke, *J. Mater. Chem. A*, 2017, **5**, 19560–19592; (b) P. Xu, N. S. McCool and T. E. Mallouk, *Nano Today*, 2017, **14**, 42–58; (c)Z. Yu, F. Li and L. Sun, *Energy Environ. Sci.*, 2015, **8**, 760–775.

3 (a) Y. Gao, X. Ding, J. Liu, L. Wang, Z. Lu, L. Li and L. Sun, *J. Am. Chem. Soc.*, 2013, **135**, 4219–4222; (b) J. W. Youngblood, S. H. A. Lee, Y. Kobayashi, E. A. Hernandez-Pagan, P. G. Hoertz, T. A. Moore, A. L. Moore, D. Gust and T. E. Mallouk, *J. Am. Chem. Soc.*, 2009, **131**, 926–927.

4 (a) A. O. Biroli, F. Tessore, G. Di Carlo, M. Pizzotti, E. Benazzi, F. Gentile, S. Berardi, C. A. Bignozzi, R. Argazzi, M. Natali, A. Sartorel and S. Caramori, *ACS Appl. Mater. Interfaces*, 2019, **11**, 32895–32908; (b) G. F. Moore, J. D. Blakemore, R. L. Milot, J. F. Hull, H. E. Song, L. Cai, C. A. Schmuttenmaer, R. H. Crabtree and G. W. Brudvig, *Energy Environ. Sci.*, 2011, **4**, 2389–2392; (c) P. K. Poddutoori, J. M. Thomsen, R. L. Milot, S. W. Sheehan, C. F. A. Negre, V. K. R. Garapati, C. A. Schmuttenmaer, V. S. Batista, G. W. Brudvig and A. Van Der Est, *J. Mater. Chem. A*, 2015, **3**, 3868–3879; (d) M. Yamamoto, Y. Nishizawa, P. Chábera, F. Li, T. Pascher, V. Sundström, L. Sun and H. Imahori, *Chem. Commun.*, 2016, **52**, 13702–13705.

5 O. Suryani, Y. Higashino, J. Y. Mulyana, M. Kaneko, T. Hoshi, K. Shigaki and Y. Kubo, *Chem. Commun.*, 2017, **53**, 6784–6787.

6 (a) F. Ronconi, Z. Syrgiannis, A. Bonasera, M. Prato, R. Argazzi, S. Caramori, V. Cristino and C. A. Bignozzi, *J. Am. Chem. Soc.*, 2015, **137**, 4630–4633; (b)J. T. Kirner and R. G. Finke, *ACS Appl. Mater. Interfaces*, 2017, **9**, 27625–27637; (c) J. T. Kirner, J. J. Stracke, B. A. Gregg and R. G. Finke, *ACS Appl. Mater. Interfaces*, 2014, **6**, 13367–13377; (d) M. Bonchio, Z. Syrgiannis, M. Burian, N. Marino, E. Pizzolato, K. Dirian, F. Rigodanza, G. A. Volpato, G. La Ganga, N. Demitri, S. Berardi, H. Amenitsch, D. M. Guldi, S. Caramori, C. A. Bignozzi, A. Sartorel and M. Prato, *Nat. Chem.*, 2019, **11**, 146–153.

7 (a) P. Bornoz, M. S. Prévot, X. Yu, N. Guijarro and K. Sivula, *J. Am. Chem. Soc.*, 2015, **137**, 15338–15341; (b) J. Chen, P. Wagner, L. Tong, G. G. Wallace, D. L. Officer and G. F. Swiegers, *Angew. Chemie - Int. Ed.*, 2012, **51**, 1907–1910; (c) J. Chen, P. Wagner, L. Tong, D. Boskovic, W. Zhang, D. Officer, G. G. Wallace and G. F. Swiegers, *Chem. Sci.*, 2013, **4**, 2797.

8 (a) F. Li, K. Fan, B. Xu, Q. Daniel, L. Sun, L. Li and E. Gabrielsson, *J. Am. Chem. Soc.*, 2015, **137**, 9153–9159; (b) K. R. Wee, B. D. Sherman, M. K. Brennaman, M. V. Sheridan, A. Nayak, L. Alibabaei and T. J. Meyer, *J. Mater. Chem. A*, 2016, **4**, 2969–2975.

9 (a) A. Coletti, S. Lentini, V. Conte, B. Floris, O. Bortolini, F. Sforza, F. Grepioni and P. Galloni, *J. Org. Chem.*, 2012, **77**, 6873–6879; (b) M. Bonomo, F. Sabuzi, A. Di Carlo, V. Conte, D. Dini and P. Galloni, *New J. Chem.*, 2017, **41**, 2769–2779; (c) F. Sabuzi, S. Lentini, F. Sforza, S. Pezzola, S. Fratelli, O. Bortolini, B. Floris, V. Conte and P. Galloni, *J. Org. Chem.*, 2017, **82**, 10129–10138; (d) F. Sabuzi, V. Armuzza, V. Conte, B. Floris, M. Venanzi, P. Galloni and E. Gatto, *J. Mater. Chem. C*, 2016, **4**, 622–629.

10 (a) A. Sartorel, N. D. McDaniel, S. Bernhard and M. Bonchio, *J. Am. Chem. Soc.*, 2008, **130**, 5006–5007; (b) J. Fielden, J. M. Sumliner, N. Han, Y. V. Geletii, X. Xiang, D. G. Musaev, T. Lian and C. L. Hill, *Chem. Sci.*, 2015, **6**, 5531–5543; (c) M. Orlandi, R. Argazzi, A. Sartorel, M. Carraro, G. Scorrano, M. Bonchio and F. Scandola, *Chem. Commun.*, 2010, **46**, 3152–3154.

11 (a) B. H. Solis and S. Hammes-Schiffer, *Inorg. Chem.*, 2014, **53**, 6427–6443; (b) D. R. Weinberg, C. J. Gagliardi, J. F. Hull, C. F. Murphy, C. A. Kent, B. C. Westlake, A. Paul, D. H. Ess, D. G. McCafferty and T. J. Meyer, *Chem. Rev.*, 2012, **112**, 4016–4093; (c) S. Hammes-Schiffer, *J. Am. Chem. Soc.*, 2015, **137**, 8860–8871; (d) J. J. Warren and J. M. Mayer, *Biochemistry*, 2015, **54**, 1863–1878.

12 (a) F. Puntoriero, S. Serroni, G. La Ganga, A. Santoro, M. Galletta, F. Nastasi, E. La Mazza, A. M. Cancelliere and S. Campagna, *Eur. J. Inorg. Chem.*, 2018, 3887–3899; (b) M. Natali, F. Nastasi, F. Puntoriero and A. Sartorel, *Eur. J. Inorg. Chem.*, 2019, 2027-2039.

13 S. Berardi, V. Cristino, M. Canton, R. Boaretto, R. Argazzi, E. Benazzi, L. Ganzer, R. Borrego Varillas, G. Cerullo, Z. Syrgiannis, F. Rigodanza, M. Prato, C. A. Bignozzi and S. Caramori, *J. Phys. Chem. C*, 2017, **121**, 17737–17745.

14 (a) K. L. Materna, R. H. Crabtree and G. W. Brudvig, *Chem. Soc. Rev.*, 2017, **46**, 6099–6110; (b) R. Brimblecombe, A. Koo, G. C. Dismukes, G. F. Swlegers and L. Spiccia, *J. Am. Chem. Soc.*, 2010, **132**, 2892–2894.

15 B. D. Sherman, M. V. Sheridan, C. J. Dares and T. J. Meyer, *Anal. Chem.*, 2016, **88**, 7076–7082.

16 C. Besson, Z. Huang, Y. V. Geletii, S. Lense, K. I. Hardcastle, D. G. Musaev, T. Lian, A. Proust and C. L. Hill, *Chem. Commun.* 2010, **46**, 2784-2786.

View Article Online DOI: 10.1039/C9CC09855D

View Article Online
DOI: 10.1039/C9CC09805D

A novel pentacyclic quinoid photosensitizer with extended absorption in the visible and enabling proton coupled electron transfer is employed in photoelectrodes for water oxidation in combination with a ruthenium polyoxometalate catalyst.